UNIVERSIDADE ESTADUAL PAULISTA
Instituto de Geociências e Ciências Exatas
Campus de Rio Claro

Gabriel Díaz Iturry

STATISTICAL INVESTIGATION AND THERMAL PROPERTIES FOR A ONE-DIMENSIONAL IMPACT SYSTEM WITH DISSIPATION

Dissertação de Mestrado apresentada ao Instituto de Geociências e Ciências Exatas do Campus de Rio Claro, da Universidade Estadual Paulista Júlio de Mesquita Filho, como parte dos requisitos para obtenção do título de Mestre em Física, área de Física Aplicada.

Orientador: Edson Denis Leonel

Rio Claro - SP
2017

311 Iturry, Gabriel Díaz
I91s Statistical investigation and thermal properties for a one-dimensional impact system with dissipation / Gabriel Díaz Iturry. - Rio Claro, 2017
45 f. : il., figs., tabs.

Dissertação (mestrado) - Universidade Estadual Paulista, Instituto de Geociências e Ciências Exatas
Orientador: Edson Denis Leonel

1. Estatística matemática. 2. Bilhares. 3. Simulação Monte Carlo. 4. Caos. 5. Modelo Bouncer unidimensional. I. Título.

Ficha Catalográfica elaborada pela STATI - Biblioteca da UNESP
Campus de Rio Claro/SP

Gabriel Díaz Iturry

STATISTICAL INVESTIGATION AND THERMAL PROPERTIES FOR A ONE-DIMENSIONAL IMPACT SYSTEM WITH DISSIPATION

Dissertação de Mestrado apresentada ao Instituto de Geociências e Ciências Exatas do Campus de Rio Claro, da Universidade Estadual Paulista Júlio de Mesquita Filho, como parte dos requisitos para obtenção do título de Mestre em Física, área de Física Aplicada.

Comissão Examinadora

Prof. Dr. Edson Denis Leonel
Prof. Dr. Iberê Luiz Caldas
Prof. Dr. Tiago Pereira da Silva

Rio Claro, 16 de fevereiro de 2017

Resultado: APROVADO

A quienes quiero.

Agradecimentos

Agradezco a mi familia por su paciencia y por el *tiempo propio* que vivimos; a mi orientador Prof. Edson Denis Leonel por el voto de confianza depositado en mi y toda la ayuda que me dió. A las amistades, antiguas y nuevas, que están ahí por el mundo. Agradezco tambien a la agencia CAPES y el departamento de Física de UNESP-Rio Claro.

A los que ayudaron en esto.

Resumo

Estudamos nessa dissertação algumas propriedades estatísticas no regime de equilibrio pós transitório para o modelo *bouncer* unidimensional considerando ambas versões completa e simplificada. O modelo consiste de uma partícula clássica movendo-se sob ação de uma força gravitacional constante e sofrendo colisões com uma plataforma móvel de massa muito maior que a massa da partícula. A versão completa leva em conta o movimento real da fronteira e o instante da colisão entre partícula e plataforma é obtido a partir da solução numérica de uma equação transcendental. Já o modelo simplificado, também conhecido como modelo de aproximação de fronteira fixa, assume que para o cálculo do instante da colisão a fronteira está parada, porém a partícula troca energia após a colisão ocorre como se a fonteira estivesse em movimento. Os comportamentos da velocidade média, velocidade quadrática média e desvio da velocidade quadrática média foram obtidos em função dos parâmetros de controle. Desenvolvemos um método semi-analítico permitindo-nos deduzir equações dos valores médios sem fazer simulações de larga escala. Em seguida, elaboramos uma simulação do tipo Monte-Carlo que nos permite obter os valores médios no estado estacionário sem resolver equações transcendentais, acelerando assim as simulações numéricas. O método de Monte-Carlo apresentado pode ser útil na investigação de sistemas mais complexos incluindo bilhares clássicos dependentes do tempo.

Palavras Chaves: Bilhares, simulação de Monte Carlo.

Abstract

We studied some statistical properties in the stationary and post transitory state for the one-dimensional bouncer model considering wither complete and simplified versions. The model consists of a classical particle moving under the effect of a constant gravitational force and collides with a periodic moving platform whose mass is heavier as compared to the particle. The complete version takes into account the real motion of the moving wall. The instant of collision is obtained from the numerical solution of a transcendental equation. The simplified version, also called as a static wall approximation, takes into account to calculate the instant of the collisions as if the wall was fixed. However, the particle experiences an exchange of energy and momentum at the collision as if the wall were moving. The behavior for the average velocity, average squared velocity and deviation of the average squared velocity were obtained as a function of the control parameters. We developed a semi-analytic method allowing us to deduce equations for the average values without the need of doing large scale simulations. Using a Monte-Carlo-like simulation we obtained the average values for the stationary state without solving the transcendental equations. The Monte-Carlo method may have applications in the investigation of more complex systems including time dependent billiard systems.

Key Words: Billiards, Monte Carlo simulation.

CONTENTS

Chapter 1

Introduction

In the mid 17th century Newton developed differential calculus. With this he was able to mathematically write the laws of movement [1] and to describe the planetary motion of two bodies, which until then were known by the empirical Kepler laws.

New generation of mathematicians and physicists tried to resolve the gravitational problem of three bodies without any success. At the end of 19th century Poincaré brought a new insight to the problem [2]. Instead of wondering about quantitative aspects he asked about qualitative aspects of the problem, as the stability of the motion. With this in mind he developed geometric approximations to analyze the problem. Even though the three body problem wasn't sovable by looking for *first integrals of motion*, at the end of 20th century Sundman found analytic series approximation of the solution to the gravitational problem of three bodies for almost all admissible initial conditions [3], later in 1990, Wang resolved the problem of n bodies [4], again in an analytic serie approximation. Both solutions showed to be of less interest than Poincaré's geometric approach for qualitative aspects, since physically they do not brought new insights in the problem in hands, even more, both series converge very slowly, so not even presented numerical improves [5].

In the second half of the 20th century the studies in dynamics focused in nonlinear oscillators and applications of those in physics and engineering, applications such as radio, laser, radar among others. In the theoretical counterpart new methods of analysis, based on Poincaré's geometric approach, were developed. The use of the computers to perform the calculations required in less time allowed to study and experiment with new equations in a way that was almost impossible before. This kind of experiments yield Lorenz, while studying atmospherics models, to the discovery of chaotic movement in strange attractors [6]. Lorenz found that the solutions to the equations he was studying could oscillate in a strange and unpredictable way, even more, starting from close initial conditions the behaviors of the trajectories could be very different between them.

After Lorenz's discovery many more similar results were found in sciences while studying nonlinear systems. In the 70's Feigenbaum realize there are universal laws governing transition between regular and chaotic behavior [7]. He proved that two completely different systems can

become chaotic in the same way. Besides chaos, nonlinear dynamics also growth due the works done in fractals and synchronization [8].

Dynamical systems provide mathematical models that helps to comprehend different phenomena [9, 10, 11, 12]. In Physics any dynamical system can be described, in principle, by a Hamiltonian. Among the variety of possible physical phenomena, the ones described by low dimensional Hamiltonian systems have a special property, they can present chaotic behavior even though the deterministic dynamics is simple.

Between all dynamical systems some of special interest are the billiards systems [13, 14], they evolve by simple dynamical rules but show all the richness of general low dimensional Hamiltonian dynamics. Even more, billiard systems can be used to model some phenomena with direct physical interpretation, as thermometric efficiency, nuclear collisions, transport [15]. The most simple one consist of a free particle moving in a N-dimensional closed region suffering collisions with a border. We can also add some special dynamics both in the original *free moving particle region* as in the *collision zone*, for example, the movement of the particle can be influenced by an external field of forces, and the border, also known as wall, is moving in a known way, besides that, the collisions can be elastic or inelastic.

The notion of billiard is known since Birkhoff proposed the problem of a spherical particle moving in many directions colliding with a border [16]. Later on, due the work of Sinai in mathematical properties of billiards of dispersing wall [17], and also Krylov's exhaustive work in the same systems [18], a new period of billiard analysis begun.

One of the branches of Physics that has been greatly benefited due to the arrival of computers is Statistical Mechanics. In this subject we are interested in calculate physical properties of condensed matter systems and others too [19]. The main problem is the need to resolve many equations of motion due the presence of many particles interacting between them and with the surrounding system. Since we are actually interested in macroscopic properties we need to take averages of a particular physical observable. In some cases the actual simulation of the many particles is realized, but in other cases is made a probabilistic simulation of the possible behavior of the system, this probabilistic style is the Monte Carlo Method [20].

The Monte Carlo Method consists of a set probabilistic rules based in some ansatzes about the behavior of a physical system. The idea of those rules is to mimic the nature of physical phenomena. Typically in Statistical Mechanics the most important ansatz is that the system achieves an equilibrium state where the energy is distributed by a Boltzmann probability. With these set of rules we perform a sampling of possible states for the system, and use those states to take expectation values of the physical observables.

The principal objective of this dissertation is to study the post-transient dynamics of the dissipative bouncer model. We focus in the mean values of physical observables related to the velocity of the bouncing particle. The main specific objectives of the dissertation are: (i) Develop a semianalytical method that allows to deduce simple equations that give the mean value of the observables of interest; (ii) Study the possibility of elaborate a Monte Carlo like

simulation to obtain the same required averages.

This work is organized as follows. In Chapter 2 we deduce the map for the Bouncer Model, we comment about how to do the simulation, we show the known results of the literature related to the averages of the particles velocity, and associated variables finally we present some results of those mean values obtained by numerical simulation. In the Chapter 3 we do an exhaustive presentation of a semianalytical method to deduce the simple equations that allow us to find analytically the mean value of different physical observables. Until this Chapter all the results are obtained both for the complete bouncer model as well as the simplified version. In Chapter 4 we introduce a more experimentally realistic bouncer model, a Stochastic-Chaotic model, that allows us to propose and elaborate a Monte Carlo like simulation letting us to calculate the average values of the observables with great accuracy. Finally, in the last Chapter we present our conclusions about the studies done in the dissertation and give our perspectives for future works.

Chapter 2

The Bouncer Model: numerical and statistical results

In this Chapter we introduce the Bouncer Model, we describe the physical phenomena behind the model, deduce and explicitly write the equations of the map for the complete and simplified versions. Then we show some results, obtained via numerical simulation, regarding physical observables related to the velocity in the steady state.

2.1 The Bouncer Model

The model studied in this dissertation is the Bouncer Model [21]. The system consists of a particle moving in one dimension under the action of a gravitational field and experiences collisions with a heavy and periodically moving wall, as illustrated in Figure 2.1.

The physics behind the problem is reduced to considering two phenomena:

1. The kinematics equation of motion for the particle and the wall are given with known initial conditions. We are interested in find where and when the particle will meet the wall in space and time. For this we need to solve the kinematic equation for t_v

$$x_p(t_v) \quad = \quad x_f(t_v), \tag{2.1}$$

this kinematic equation means that for a given time t_v the position of the particle, x_p, and the border, x_f, is the same. Both positions may depend on some parameters and initial conditions. In general the kinematic equation (2.1) can be difficult to solve since it can take the expression of a transcendental equation with many mathematical solutions for t_v. Physically we are interested in the mathematical solution that gives the least positive t_v, otherwise the particle traversed the wall corresponding to a nonphysical solution.

2. The velocity of both the particle and the wall are given in the instant before the impact. We are interested in know what is the velocity of the particle right after the impact. Here

we consider that the wall is infinitely heavy as compared to the particle and the collision is inelastic, which means a fractional loss of energy upon collision. The collision equation is

$$V_1 - V_f = -\gamma (V_0 - V_f), \tag{2.2}$$

where V_0 and V_1 are the particle's velocity, before and after the collision respectively, V_f is the wall's velocity at the moment of the impact, and γ is the dissipation parameter that ranges between 0 (plastic collision) and 1 (elastic collision). Equation (2.2) comes from the analysis of the collision in the wall's Galilean referential frame, where the particle's velocity changes as $V_1' = -\gamma V_0'$ at the collision.

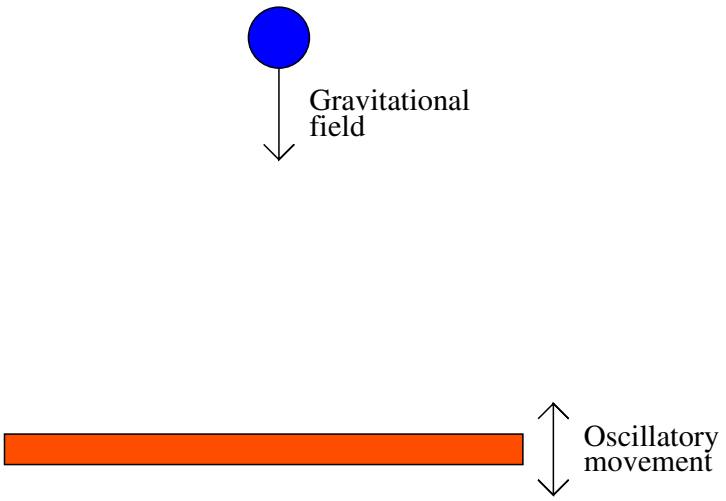

Figure 2.1: Representation of the Bouncer Model: a particle moving in a gravitational field and colliding with an oscillating wall.

The dynamics of the bouncer system is described by a two-dimensional, non-linear discrete mapping for the two variables velocity of the particle v and time t immediately after the n^{th} collision of the particle with the moving wall. The investigations are made based on two main versions of the model: *(i)* complete, which takes into account the whole movement of the oscillating border; and *(ii)* a static wall approximation, also called simplified version [22], where the wall is static but at the moment of the collision there can be an exchange on energy and momentum as if the wall were moving. Besides, the collision is considered inelastic.

2.1.1 Complete bouncer model

To construct the complete mapping we consider that the motion of the border is described by

$$x_f(t) = \varepsilon \cos(\omega t), \tag{2.3}$$

where ε and ω are parameters that give the amplitude of the wall's oscillation and it's frequency of movement respectively.

The motion of the particle is uniformly accelerated, its general equation is

$$x_p(t) = x_0 + v_0 t - \frac{gt^2}{2}, \tag{2.4}$$

where x_0 and v_0 are the particle's initial position and velocity, g is the acceleration due the gravitational field, which we assume as constant.

If we consider that a collision between the moving platform and the particle happened at the instant of time t_0, so $x_p(t_0) = x_f(t_0) = \varepsilon \cos(\omega t_0)$, the kinematic equation (2.1) that we need to solve in order to find the position and time of the next collision is

$$\varepsilon \cos(\omega t_0) + v_0 t_v - \frac{g t_v^2}{2} - \varepsilon \cos(\omega [t_v + t_0]) = 0, \tag{2.5}$$

where the velocity of the particle after the first collision, v_0, is assumed to be known. Solving for t_v we find the time between collision. With this we can calculate when the next collision happens, $t_1 = t_0 + t_v$, and the position $x_f = \varepsilon \cos(\omega [t_0 + t_v])$.

With the time of flight t_v we can also calculate the velocity of the particle after the collision, Eq. (2.2):

$$v_1 = -\gamma (v_0 - g t_v) - (1+\gamma)\varepsilon\omega \sin(\omega [t_v + t_0]). \tag{2.6}$$

Since the problem has four parameters (g, ω, ε, γ) and two basic physical magnitudes (interval of time and distance), we can work with dimensionless variables reducing the number of parameters to only two. Working in Equations (2.5) and (2.6) we get

$$\begin{aligned}
\left(\frac{\omega^2\varepsilon}{g}\right)\cos(\omega t_0) + \left[\frac{\omega}{g}v_0\right][\omega t_v] - \frac{[\omega t_v]^2}{2} - \left(\frac{\omega^2\varepsilon}{g}\right)\cos([\omega t_v + \omega t_0]) &= 0, \\
-\gamma\left(\left[\frac{\omega}{g}v_0\right] - [\omega t_v]\right) - (1+\gamma)\left(\frac{\omega^2\varepsilon}{g}\right)\sin([\omega t_v + \omega t_0]) &= \left[\frac{\omega}{g}v_1\right],
\end{aligned}$$

doing the following changes of variables $\omega t \mapsto \phi$, $\frac{\omega}{g} v \mapsto V$, $\frac{\omega^2\varepsilon}{g} \mapsto \epsilon$ we have the following map for the $(n+1)^{th}$ collision:

$$V_{n+1} = -\gamma (V_n - t_v) - (1+\gamma)\epsilon \sin(\phi_{n+1}), \tag{2.7}$$

$$\phi_{n+1} \;=\; (\phi_n + t_v)\, mod\, (2\pi)\,,$$

with help of the transcendental equation for the dimensionless t_v variable

$$\epsilon\left(\cos\left(\phi_n + t_v\right) - \cos\left(\phi_n\right)\right) - V_n t_v + \frac{t_v^2}{2} \;=\; 0. \tag{2.8}$$

We recognize that ϵ is the nonlinear parameter since it causes the dynamics to be complex when it is different of 0 and trivial otherwise.

Solving equation (2.8) is not easy since it is a transcendental equation without analytic solution. Even more, this equation can have many mathematical solutions due the oscillatory function $\cos(t)$. From all solutions for t_v, we are interested in the smallest positive one since physically means the time of flight between successive collisions. Numerically we usually find this time by molecular dynamics, we add an small interval of time, Δt, to t_n and ask whether the particle's position is lower than the walls position. If so, we have an approximation of the time $t_v = t_0 + \Delta t$, if not, we increase the interval of time and ask again. With the approximate value of t_v we can find a better result by using any numerical method, as bissection or Raphson-Newton, to solve equation (2.8). It is worth to emphasize that both the initial Δt and the numerical method used must be tested to find if we converge to the actual physical solution.

Figure 2.2 (a) shows the phase space for $\epsilon = 0.5$ and $\gamma = 1$. It can be seen the mixed dynamics scenario, typical of conservative Hamiltonian systems, containing stability islands and chaotic seas. In Figure 2.2 (c) the islands become small and there is almost a single chaotic sea where the velocity *diffuses* to infinity in the phenomenon known as Fermi Acceleration [23].

Introducing dissipation destroys the mixed structure of phase space. As shown in Figure 2.2 (b) for $\epsilon = 0.5$ and $\gamma = 0.99$, the dense clouds of points suggest the presence of attractors in plane space producing a very complex dynamics. Finally, Figure 2.2 (d) shows that the plane space can be considered as composed by just one chaotic attractor that suppresses the Fermi Acceleration phenomenon [24, 25].

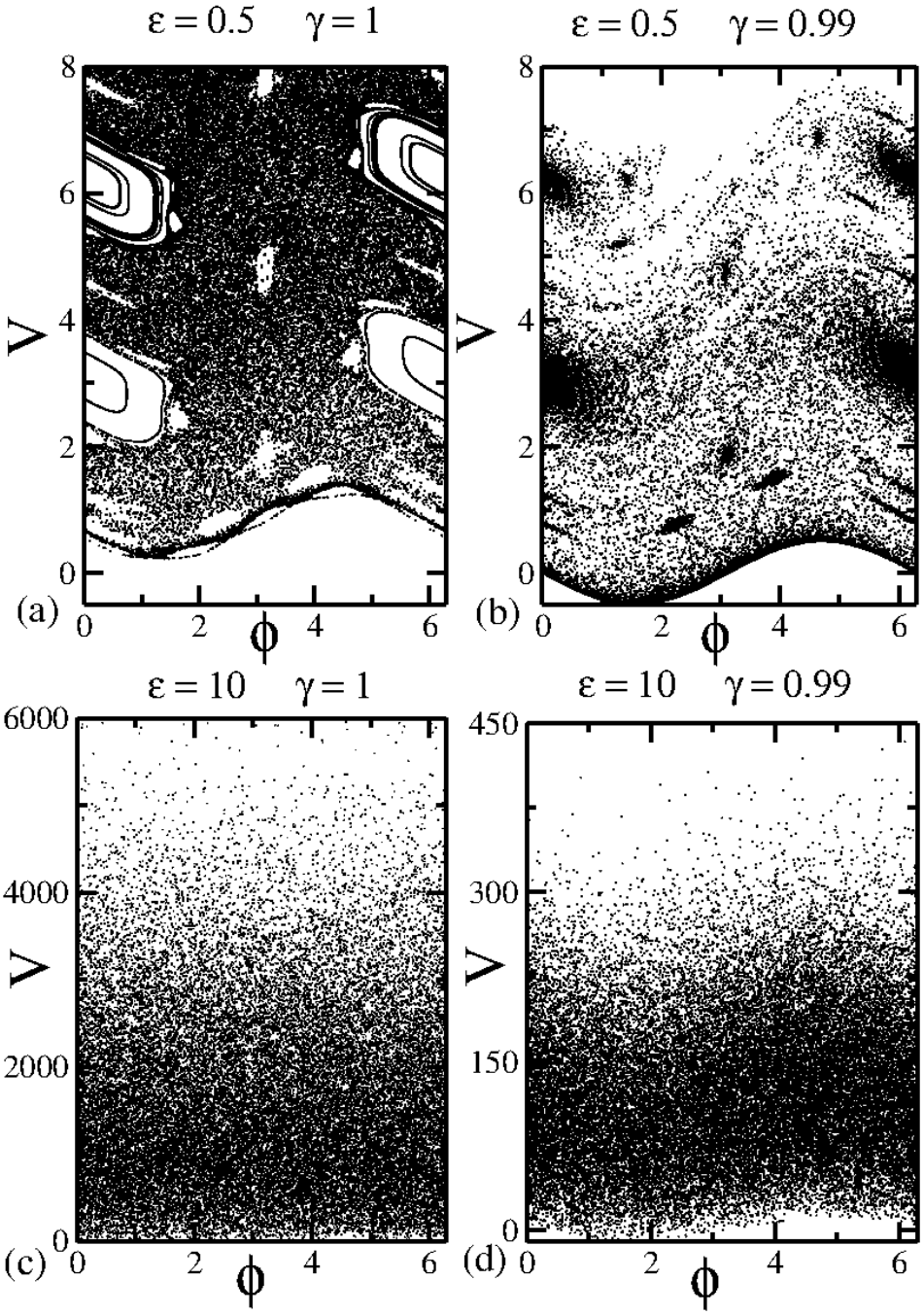

Figure 2.2: In (a) and (c) a representation of the phase space for the complete bouncer model considering non-dissipative dynamics. The control parameters used were: (a) $\epsilon = 0.5$ and $\gamma = 1$; (c) $\epsilon = 10$ and $\gamma = 1$. In (b) and (d) are a snapshot of the trajectories in the phase plane for the dissipative dynamics. The parameters used were: (b) $\epsilon = 0.5$ and $\gamma = 0.99$; (d) $\epsilon = 10$ and $\gamma = 0.99$.

To specify the dynamics of the particle/wall we need to know the pair (ϕ_n, V_n), which gives the current state of the system. This pair can be represented in the *plane space* (ϕ, V) as a point. The evolution over time of (ϕ_n, V_n) makes a trajectory, while its evolution over infinity time towards future as well as past makes the orbit of the particle. The *phase space* is the set of all possible trajectories after discharging the transient motion, if any.

In the phase space periodic orbits exist. If those periodic orbits have elliptical stability, *i. e.*, the stability matrix has purely imaginary eigenvalues, a special kind of orbits will form around them. This kind of orbits can be view as a multiple periodic orbit with nonconmensourable periods. The set of these kind of orbits are known as an invariant tori, or also as *stability islands*. Around the stability islands exist a different kind of orbits which behave in a very irregular way, in the sense that initially close trajectories will diverge in small amount of time but will mix again and again in some future random interval of time. The set of this orbits form the *chaotic sea*. When the phase space shows both stability islands as well as a chaotic sea we say that there is a *mixed dynamics*.

In certain Billiard systems, when starting an ensemble of initial conditions, the mean energy of the ensemble grows without a upper bound. If this behavior is found we say that the billiard presents *Fermi acceleration*.

When the dissipation is present in a system the elliptic periodic orbits become puntual attractors due the fact that the stability matrix now has eigenvalues with absolute values less than the unity. More complicated types of atractors also exist, including the locking attractor with the wall, when the particle is *glued* to the border. An *attractor* is the minimal set of orbits that always stays in a bounded region of the plane space, and trajectories near this region become closer to it when time pases. If the orbits in the attractor behave in the irregular way, in the sence defined above, we say that the orbits are in a *chaotic attractor*.

The Jacobian matrix is given by:

$$J = \begin{pmatrix} \frac{\partial V_{n+1}}{\partial V_n} & \frac{\partial V_{n+1}}{\partial \phi_n} \\ \frac{\partial \phi_{n+1}}{\partial V_n} & \frac{\partial \phi_{n+1}}{\partial \phi_n} \end{pmatrix}, \tag{2.9}$$

where V_{n+1} and ϕ_{n+1} are given by the mapping equations (2.7) and (2.8). It can be shown that the determinant of the Jacobian matrix is

$$\det[J] = \gamma^2 \left[\frac{V_n + \epsilon \sin(\phi_n)}{V_{n+1} + \epsilon \sin(\phi_{n+1})} \right]. \tag{2.10}$$

From last equation two facts immediatly deserve our attention:

1. When $\gamma = 1$, conservative dynamics, the determinant of the Jacobian matrix is different from 1. This is due the fact that we are not working in canonical variables. However, there is a measure that is preserved, *i. e.*, $d\mu = (V + \epsilon \sin(\phi))\, dV d\phi$.

2. When $\gamma < 1$, dissipative dynamics, the measure $d\mu$ is not preserved anymore.

The consequences of the second fact are not easely seen. To understand this repercussions we have to work with the conservative dynamics. We will first look for canonical variables to work, specifically we will focus in the position, x_n, and velocity, V_n, of the particle.

The Jacobian matrix, (2.9), gives us the behavior, from one collision to the next, of infinitesimaly close trajectories starting immediately after the n^{th} collision. We want to find a

stability matrix that gives us the behavior of infinitesimaly close trajectories starting at the same instant of time when working in the canonical variables selected. To do this we recall that the infinitesimaly close trajectories after the n^{th} collision have different positions in phase plane

$$\begin{aligned} V_n' &= V_n + \Delta V_n, \\ \phi_n' &= \phi_n + \Delta\phi_n, \\ x_n' &= x_n - \epsilon \sin(\phi_n)\, \Delta\phi_n, \end{aligned}$$

where ΔV_n and $\Delta\phi_n$ stand for the infinitesimaly variations in the velocity and phase between the trajectories after the n^{th} collision. The position and velocity *at the same instant of time* are

$$\begin{aligned} V_n'' &= (V_n + \Delta V_n) - (-\Delta\phi_n), \\ x_n'' &= x_n - \epsilon \sin(\phi_n)\, \Delta\phi_n + (V_n + \Delta V_n)(-\Delta\phi_n) - \frac{(-\Delta\phi_n)^2}{2}, \end{aligned}$$

and the variations δV_n and δx_n of positions, at the same instant of time, of infinitesimaly close trajectories are

$$\begin{pmatrix} \delta V_n \\ \delta x_n \end{pmatrix} = \begin{pmatrix} 1 & 1 \\ 0 & -\epsilon \sin(\phi_n) - V_n \end{pmatrix} \begin{pmatrix} \Delta V_n \\ \Delta\phi_n \end{pmatrix}. \tag{2.11}$$

Recalling that

$$\begin{pmatrix} \Delta V_{n+1} \\ \Delta\phi_{n+1} \end{pmatrix} = J[V_n, \phi_n] \begin{pmatrix} \Delta V_n \\ \Delta\phi_n \end{pmatrix}, \tag{2.12}$$

where $J[V_n, \phi_n]$ is given by equation (2.9). Then we arrive at

$$\begin{aligned} \begin{pmatrix} \delta V_{n+1} \\ \delta x_{n+1} \end{pmatrix} &= \begin{pmatrix} 1 & 1 \\ 0 & -\epsilon \sin(\phi_{n+1}) - V_{n+1} \end{pmatrix} J[V_n, \phi_n] \begin{pmatrix} 1 & 1 \\ 0 & -\epsilon \sin(\phi_n) - V_n \end{pmatrix}^{-1} \begin{pmatrix} \delta V_n \\ \delta x_n \end{pmatrix} \\ &= J[V_n, x_n] \begin{pmatrix} \delta V_n \\ \delta x_n \end{pmatrix}, \end{aligned} \tag{2.13}$$

with this we get

$$\det[J[V_n, x_n]] = 1, \tag{2.14}$$

Using this last result now we can analyze the consequences of the dissipative dynamics. Since $\det[J] = \gamma^2 < 1$ there will be contraction of the area in the phase plane and trajectories will give rise to attractors, even more, there will be a supression of Fermi acceleration.

2.1.2 Simplified bouncer model

In the simplified version, also known as static wall approximation, the time of flight is easily calculated since the platform is considered static, the kinematic equation (2.1) of motion is

$$0 = v_0 t_v - \frac{g t_v^2}{2}, \tag{2.15}$$

and the time of flight is given by $t_v = 2\frac{v_0}{g}$. The collision equation (2.2) does consider that the wall is moving

$$v_1 = -\gamma\left(v_0 - g\left[2\frac{v_0}{g}\right]\right) - (1+\gamma)\,\varepsilon\omega\sin\left(\omega\left[t_0 + \left[2\frac{v_0}{g}\right]\right]\right). \tag{2.16}$$

Rewriting equation (2.16) in a more convenient way we obtain

$$\left[\frac{\omega}{g}v_1\right] = \gamma\left[\frac{\omega}{g}v_0\right] - (1+\gamma)\left(\frac{\omega^2\varepsilon}{g}\right)\sin\left(\left[\omega t_0 + 2\left[\frac{\omega}{g}v_0\right]\right]\right).$$

Again making $\omega t \mapsto \phi$, $\frac{\omega}{g}v \mapsto V$, $\frac{\omega^2\varepsilon}{g} \mapsto \epsilon$, the map for the dimensionless variables V_n, ϕ_n in the static wall approximation is:

$$\begin{aligned} V_{n+1} &= \left|\gamma V_n - (1+\gamma)\,\epsilon\sin\left(\phi_{n+1}\right)\right|, \\ \phi_{n+1} &= \left(\phi_n + 2V_n\right) mod\left(2\pi\right), \end{aligned} \tag{2.17}$$

where the absolute value function was introduced in order to avoid the physical incongruence of negative velocities solutions, meaning that the particle traversed the wall during the collision.

Similar as Figure 2.2, Figure 2.3 shows mixed structure, including coexistence of chaotic and regular motion, and energy diffusion for $\gamma = 1$, while for the dissipative case, $\gamma = 0.99$, attractors exist. When V is near 0 we see that the phase space differs a lot from the complete model. This behavior is due the absolute value. It produces an abrupt cut in $V = 0$, while the complete version does not have that. Its minimum value for velocity behaves like $\sin(\phi)$, without any suddenly change, this behavior will have consequences in the probability distribution for the velocities as we will see later in Chapter 3.

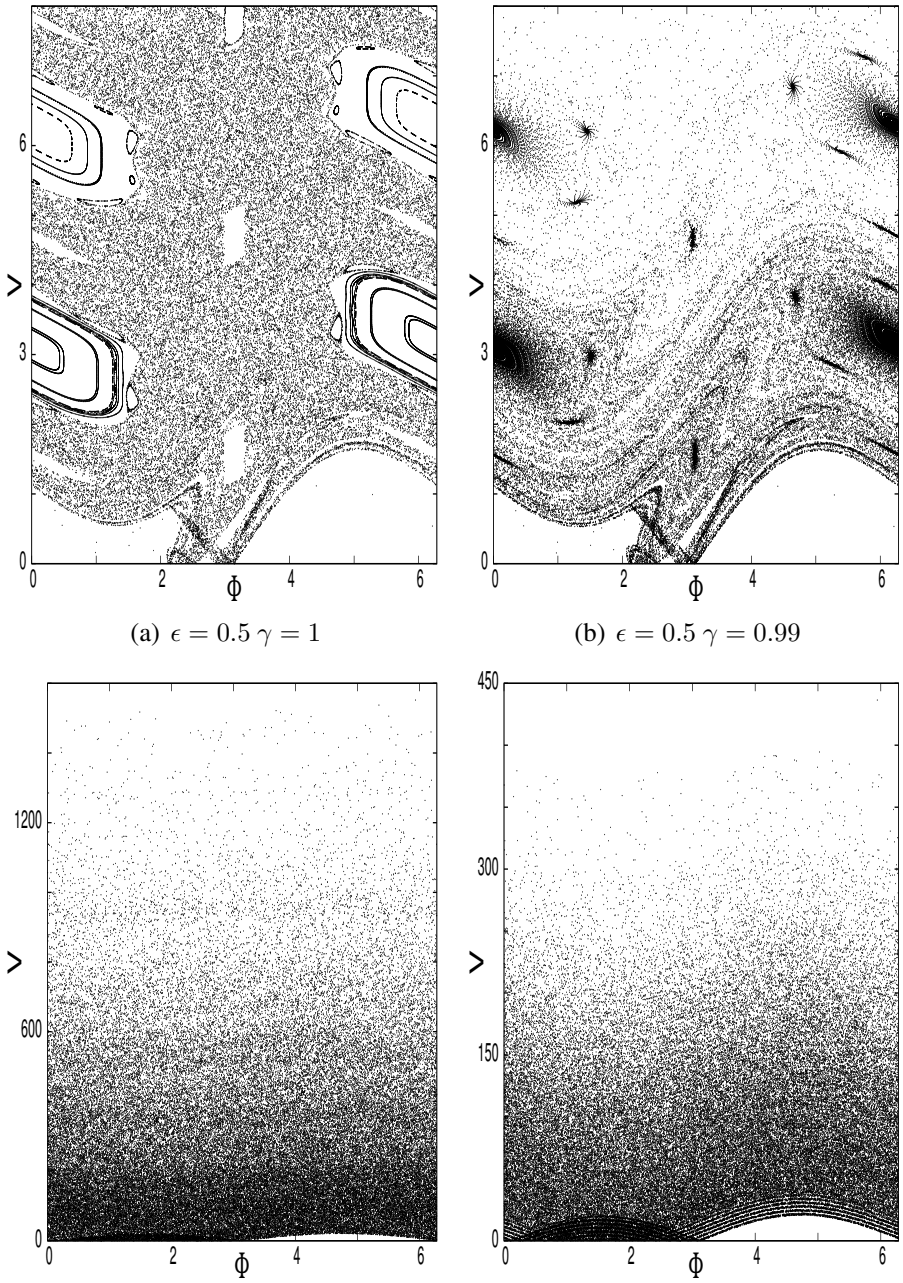

(a) $\epsilon = 0.5\ \gamma = 1$ (b) $\epsilon = 0.5\ \gamma = 0.99$

(c) $\epsilon = 10\ \gamma = 1$ (d) $\epsilon = 10\ \gamma = 0.99$

Figure 2.3: In (a) and (c) a representation of the phase space for the complete bouncer model considering non-dissipative dynamics. The control parameters used were: (a) $\epsilon = 0.5$ and $\gamma = 1$; (c) $\epsilon = 10$ and $\gamma = 1$. In (b) and (d) are a snapshot of the trajectories int the phase plane for the dissipative dynamics. The parameters used were: (b) $\epsilon = 0.5$ and $\gamma = 0.99$; (d) $\epsilon = 10$ and $\gamma = 0.99$.

2.2 Numerical and statistical results

Because we have the dynamical equations of the mappings, (2.7) and (2.8) for the complete version and (2.17) for the simplified one, different statistical investigations can be made using different types of averages.

An observable which is immediate is the average velocity measured along the orbit. It is written as

$$\overline{V_i} = \frac{1}{n}\sum_{j=1}^{n} V_j. \tag{2.18}$$

We can use last equation and average it over an ensemble of different initial conditions, hence leading to

$$\langle V \rangle = \frac{1}{M}\sum_{i=1}^{M} \overline{V_i}, \tag{2.19}$$

where M represents the number of initial conditions of the ensemble. The root mean square velocity is obtained as

$$V_{rms} = \sqrt{\langle V^2 \rangle}. \tag{2.20}$$

The deviation around the average velocity, ω, is obtained from

$$\omega = \sqrt{\langle V^2 \rangle - \langle V \rangle^2}. \tag{2.21}$$

As it is known, for large ϵ and $\gamma = 1$, unlimited diffusion in velocity can be observed. Because of the dissipation, the unlimited diffusion is not allowed anymore. The average dynamics, no mater the initial velocity, will converge to an asymptotic state for large time. If the initial condition is large, the time average velocity of the particle decreases until reaches the stationary state [26, 27]. In opposite way, starting with small initial velocity the dynamics leads the time average velocity to experience an initial growth and then achieve a constant plateau. If the initial velocity is neither small or large, say below the saturation regime, an additional crossover time is observed in the curves [28, 29]. The average velocity of the particle at the stationary regime depends both on the nonlinear parameter ϵ as well on the dissipation parameter γ as $\epsilon^1 \left(1-\gamma\right)^{-1/2}$ [24, 25].

Based on the posed above, we show in Figure 2.4 the behavior of $\langle V \rangle$ (black circles and squares), V_{rms} (red up and down triangles) and ω (blue right and left triangles) as function of the number of collisions n. The initial velocities were chosen in two different regimes: (i) high initial velocities ($V_0 \approx 10^3\epsilon$) and; (ii) low initial velocities ($V_0 \approx \epsilon$). We ensemble average the dynamics by considering the phase was uniformly distributed in the range $\phi \in [0, 2\pi]$.

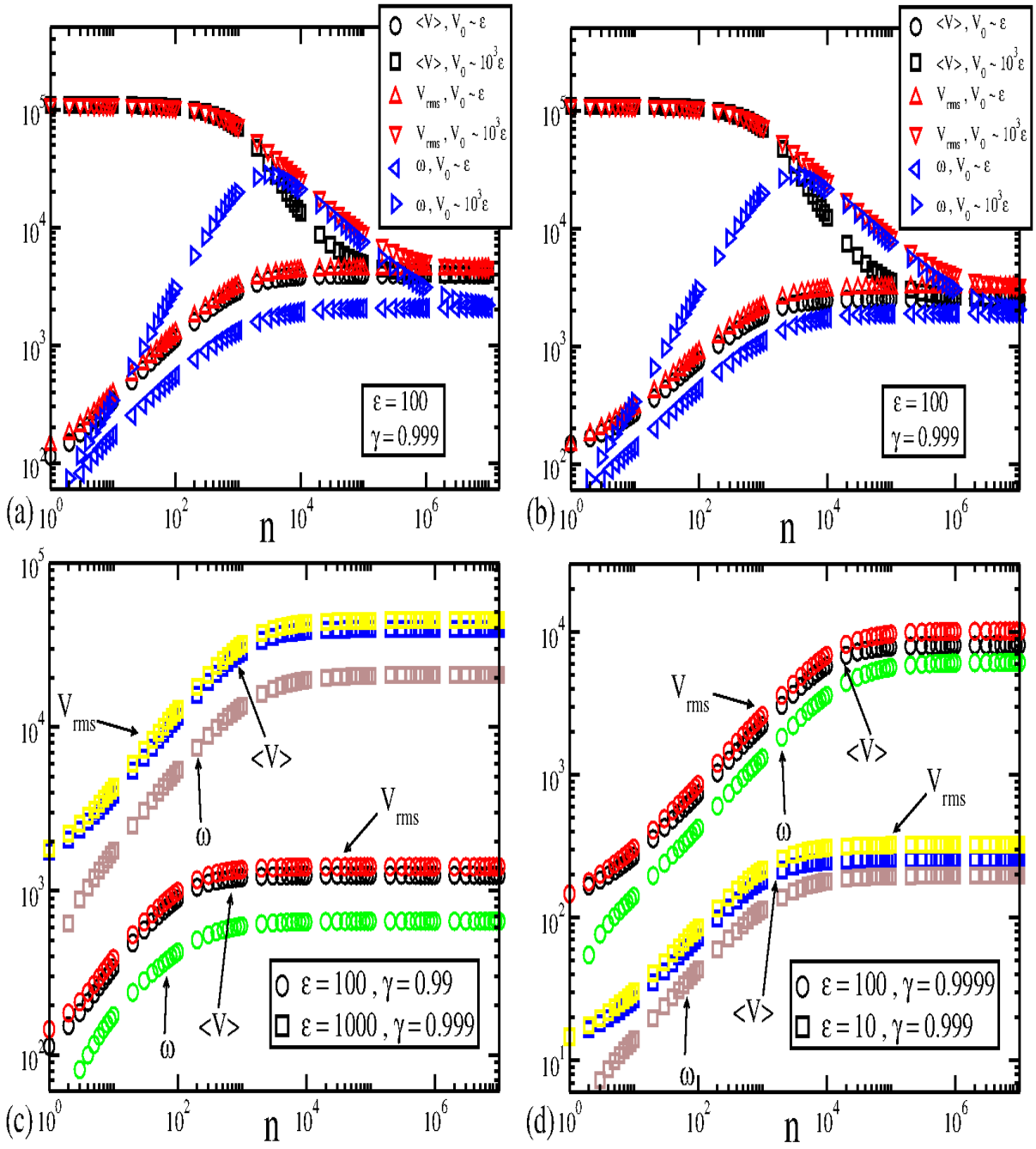

Figure 2.4: Evolution of $\langle V \rangle$, V_{rms} and ω as function of n. The control parameters are shown in the figure. Complete in (a) and static wall approximation in (b) show the dynamics considering either small and large initial velocities. Small initial conditions are considered in (c) an (d), for the complete and static wall approximation. All curves show a convergence to the stationary state for long times.

A comparison of the saturation of the three observables $\langle V \rangle$, V_{rms} and ω is better seen in Figure 2.4 (c,d). Important to mention is that a change in the parameter ϵ leads to different saturation and it does not affect the crossover time. However, the parameter γ changes both the saturation (stationary state) and the crossover times. With a scaling approach a rescale can be done and overlap both curves, of the same observable, into an universal plot.

The numerical values of the saturation plateaus for different values of the control parameters are shown in Tables 2.1 and 2.2. We see the saturation plateaus for the complete version are higher as compared to the static wall approximation. This is close connected to the probability distribution function of the velocity in the phase space. For short, the particle *prefers* to stay with high energy in the complete version while compared to the static wall approximation. Although the phase space is similar for both versions, their occupation are different.

ϵ	γ	$\langle V \rangle$	V_{rms}	ω
10	0.999	257.54(5)	324.30(5)	197.09(2)
100	0.99	793.85(4)	995.03(5)	599.91(3)
100	0.999	2531.2(3)	3165.9(5)	1901.5(4)
100	0.9999	8091(9)	10079(9)	5999(9)
1000	0.999	25222(4)	31611(5)	19054(2)

Table 2.1: Simplified mapping: Numerical values for the stationary state for $\langle V \rangle$, V_{rms} and ω considering some pairs of (ϵ, γ).

ϵ	γ	$\langle V \rangle$	V_{rms}	ω
10	0.999	407.50(4)	461.23(4)	216.05(1)
100	0.99	1244.3(1)	1405.6(1)	653.53(3)
100	0.999	3959.7(2)	4469.0(3)	2071.7(2)
100	0.9999	12736(4)	14333(8)	6570(9)
1000	0.999	39608(1)	44694(2)	20706(1)

Table 2.2: Complete mapping: Numerical values for the stationary state for $\langle V \rangle$, V_{rms} and ω considering some pairs of (ϵ, γ).

Chapter 3

Analitycal thermodynamical results

In this Chapter we describe some thermodynamical results for the proposed models by an analytical method motivated by Ref. [30]. After taking some considerations from numerical results, we propose a method to find analytically the mean value of different physical observables in the post-transient regime of the dynamics. We first present our results for the simplified version, Equations (2.17) and then for the complete version, Equations (2.7) and (2.8).

3.1 Simplified version

To describe some of the thermodynamical properties for the simplified model, we use the equations of motion (2.17) considering many different trajectories. We iterate the mapping equations, discard the transient dynamics, and then we construct an percentage histogram for the velocity variable, as an attempt to have an insight of the probability density function for the velocity.

From Figure 3.1 (a) we see that the histogram for the velocity has a half-Gaussian shape around zero. Such shape allows us to write the probability density function for the velocity as a function of the type $\rho_S(V) = \frac{2}{\sqrt{2\pi}\sigma} e^{-\frac{V^2}{2\sigma^2}}$ for $V \in [0, \infty)$. Also, we see in Figure 3.2 (a) that the distribution probability for the phase variable is almost uniform, and can be shown numerically that is nearly independent of the velocity variable, so the averages can be taken separately for each variable. Therefore, the mean squared velocity is given by

$$\left\langle V^2 \right\rangle = \int_0^\infty V^2 \rho_S(V)\, dV = \sigma^2. \tag{3.1}$$

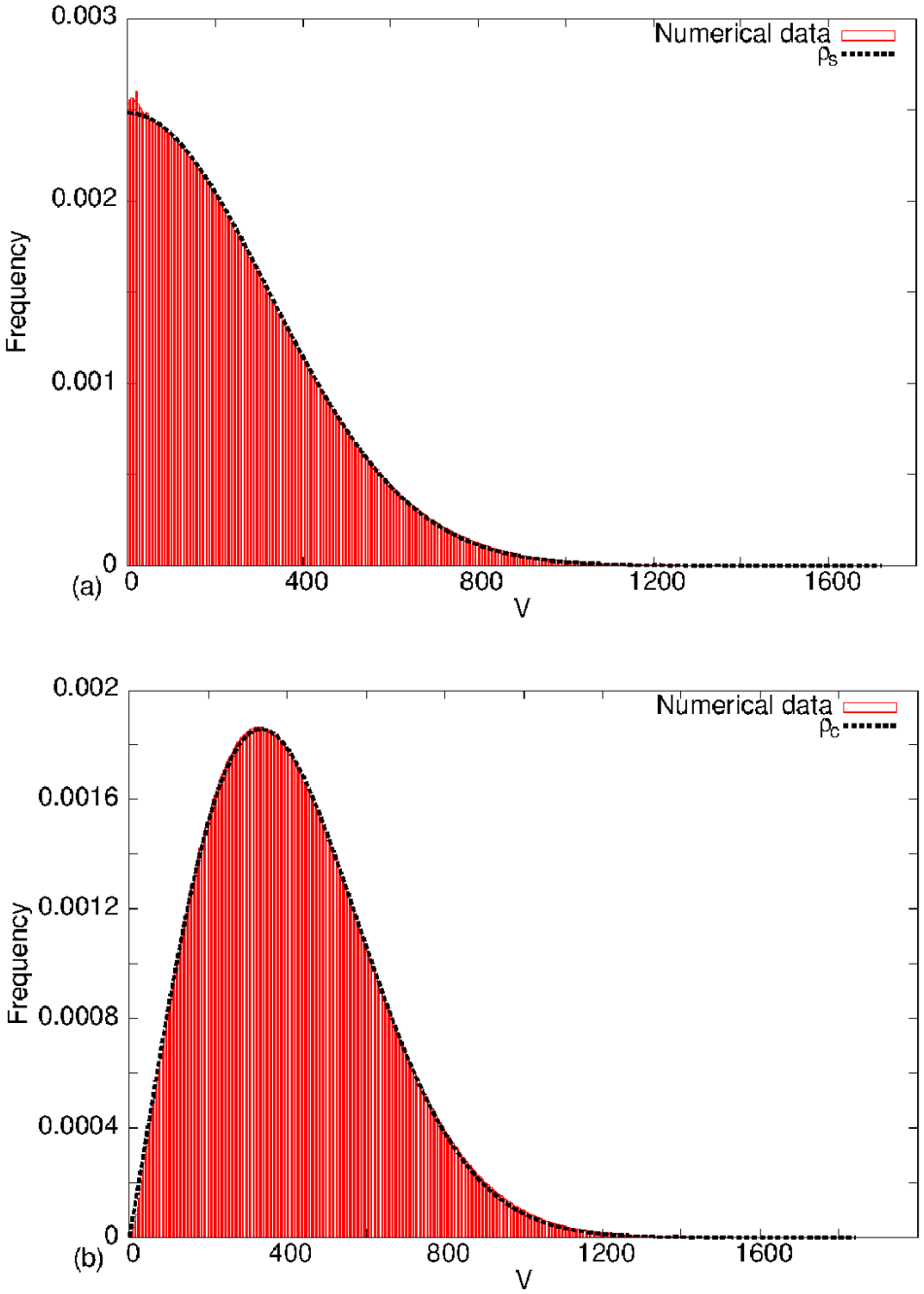

Figure 3.1: Percentage histogram and probability distribution function for: (a) a simplified version, (b) complete version of the impact system.

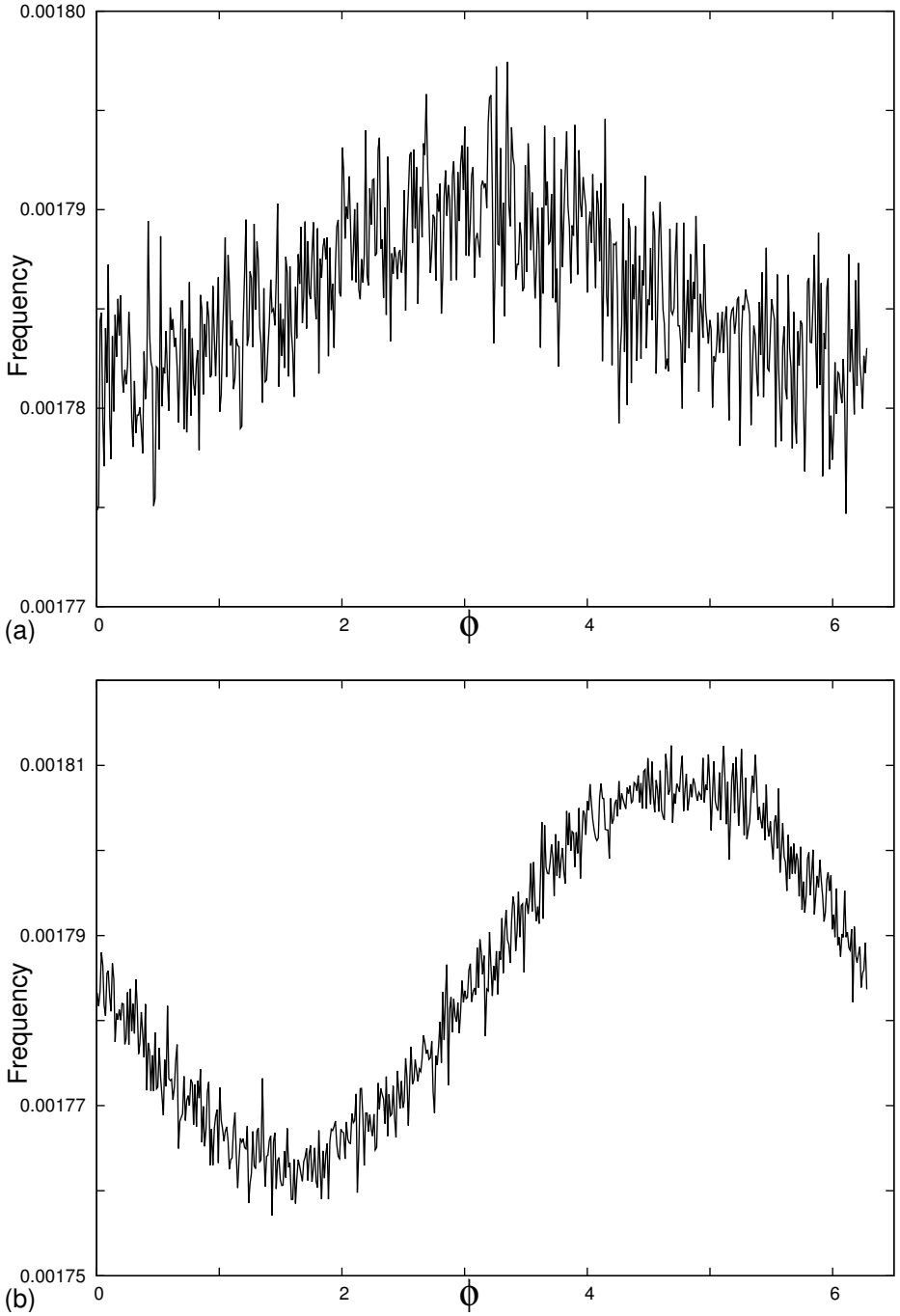

Figure 3.2: Percentage histogram of ϕ variable, V value in a small interval, for: (a) a simplified version, (b) complete version of the impact system. We see that in both versions the size of the maximum value minus the least value in the vertical axis is of order 0.01 compared to the mean value in the same axis, so the distribution for the phase variable can be considered uniform.

It is known that for an ideal classical gas the temperature is proportional to the mean kinetic energy. Hence, we choose $T = \sigma^2$and straightforward integration yields

$$\langle V \rangle \;=\; \sqrt{\frac{2T}{\pi}}. \tag{3.2}$$

The expression for the temperature can also be obtained directly from the mapping (2.17). Squaring both sides of the expression for the velocity and taking the average over an ensemble of different initial phases $\phi \in [0, 2\pi]$, we end up with

$$\left\langle V_{n+1}^2 \right\rangle = \gamma^2 \left\langle V_n^2 \right\rangle_V + \frac{(1+\gamma)^2 \epsilon^2}{2}. \tag{3.3}$$

Here the first term on the right side of the equation is averaged over the velocity probability distribution and the second term is obtained after averaging over the phase variable. At the stationary state, and considering the result of Equation (3.1), we have $T = \gamma^2 T + \frac{(1+\gamma)^2\epsilon^2}{2}$, thus yielding

$$T = \frac{(1+\gamma)\epsilon^2}{2(1-\gamma)}. \tag{3.4}$$

The other quantities can also be obtained by a similar procedure, as the one done in Equation (3.1), in particular the root mean square velocity

$$\sqrt{\langle V^2 \rangle} = \sqrt{T}, \tag{3.5}$$

and also the deviation around the mean velocity

$$\omega = \sqrt{\left(1 - \frac{2}{\pi}\right) T}. \tag{3.6}$$

Using Equations (3.2), (3.5), (3.6) and the temperature given by equation (3.4) it is possible to recover the same numerical values for $\langle V \rangle$, V_{rms} and ω shown in Table 2.1, see Table 3.1.

3.2 Complete model

Now we discuss the results for the complete model, proceeding in similar way as made to the simplified version. Figure 3.1 (b) shows that the probability distribution can be approximated by a Weibull distribution [31] with shape parameter $k = 2$. The probability distribution function is then written as $\rho_C(V) = \frac{V}{T} e^{-\frac{V^2}{2T}}$, and we consider in our calculations that $V \in [0, \infty)$. In fairness, the real variation of velocity is $[-\epsilon, \infty)$ but the probability of finding a velocity in the interval $[-\epsilon, 0)$ is very small compared to the complementary range for the parameters considered in this work. In this case, we can also see in Figure 3.2 (b) that the distribution probability for the phase variable is almost uniform, and can be shown numerically that is

practically independent of the velocity variable. From such distribution we have

$$\langle V \rangle \;=\; \sqrt{\frac{\pi T}{2}}. \tag{3.7}$$

To discuss the temperature in terms of the dynamical equations, it turns convenient to rewrite the transcendental equation (2.8) in a more convenient way as

$$-V_n t_v + \frac{t_v^2}{2} + m\epsilon\left(\cos\left(\phi_n + t_v\right) - \cos\left(\phi_n\right)\right) \;=\; 0. \tag{3.8}$$

The parameter m is defined in such way that for $m = 0$ the results for the simplified version are obtained. For $m = 1$we consider the complete version, while for $0 < m < 1$ the solution for t is required. Suppose t can be approximated by

$$t_v \;=\; a_0 + a_1 m + a_2 m^2 + a_3 m^3 + \ldots \tag{3.9}$$

for $0 \leq m \leq 1$. Replacing eq. (3.9) in the expression (3.8), after some straightforward algebra and rearranging properly the terms, we have

$$\begin{aligned} \left[\frac{a_0^2}{2} - V_n a_0\right] + \left[a_0 a_1 - V_n a_1 - \epsilon\cos\left(\phi_n\right) + \epsilon\cos\left(\phi_n + a_0\right)\right] m \\ + \left[a_0 a_2 - V_n a_2 + \frac{a_1^2}{2} - \epsilon\sin\left(\phi_n + a_0\right) a_1\right] m^2 \\ + \left[a_0 a_3 - V_n a_3 + a_1 a_2 - -\epsilon\sin\left(\phi_n + a_0\right) a_2 - \frac{\epsilon\cos\left(\phi_n + a_0\right)}{2} a_1^2\right] m^3 \;=\; 0. \end{aligned} \tag{3.10}$$

We truncate eq. (3.10) at the third term and obtain the expressions for $a_0\left[V\right]$, $a_1\left[V,\phi\right]$, $a_2\left[V,\phi\right]$ and so on, considering that each element inside of the brackets must vanish. The relations for $a_0\left[V\right]$, $a_1\left[V,\phi\right]$, $a_2\left[V,\phi\right]$ are

$$\begin{aligned} a_0 &= 2V_n, \\ a_1 &= \frac{\epsilon\left(\cos\left(\phi_n\right) - \cos\left(\phi_n + a_0\right)\right)}{a_0 - V_n}, \\ a_2 &= \frac{\epsilon\sin\left(\phi_n + a_0\right) a_1 - \frac{a_1^2}{2}}{a_0 - V_n}. \end{aligned} \tag{3.11}$$

From numerical simulations we known that the probability of $V \leq \epsilon$ is small, hence $\frac{|a_{g+1}|}{|a_g|} < 1$ then the series converges for $0 \leq m < 1$.

Using eq. (3.9) and the expressions given in (3.11), at the equilibrium state we have

$$\begin{aligned}\langle V_{n+1}\rangle &= \left[\gamma\langle V_n\rangle-(1+\gamma)\,\epsilon\langle\sin(\phi_n+2V_n)\rangle\right]+\left[\gamma\langle a_1\rangle-(1+\gamma)\,\epsilon\langle\cos(\phi_n+2V_n)\,a_1\rangle\right]m\\ &+\left[\gamma\langle a_2\rangle-(1+\gamma)\,\epsilon\left\langle\cos(\phi_n+2V_n)\,a_2-\frac{\sin(\phi_n+2V_n)}{2}a_1^2\right\rangle\right]m^2. \qquad (3.12)\end{aligned}$$

The terms $\langle\sin(\phi_n+2V_n)\rangle$ and $\langle a_1\rangle$ have zero value after averaging over the phase variable, which is distributed uniformly. Also, one can realize that $\langle\cos(\phi_n+2V_n)\,a_1\rangle=\left\langle\frac{\epsilon}{V_n}\cos(\phi_n+2V_n)\right.$ $\left.(\cos(\phi_n)-\cos(\phi_n+2V_n))\right\rangle$. After take an average over the phase , one can obtain

$$\langle\cos(\phi_n+2V_n)\,a_1\rangle = \left\langle\frac{\epsilon}{2V_n}(\cos(2V_n)-1)\right\rangle_V, \qquad (3.13)$$

where the right-hand side term can be expressed by the cosine function expansion as

$$\langle\cos(\phi_n+2V_n)\,a_1\rangle = \epsilon\left\langle\sum_{l=0}^{\infty}\frac{(-1)^{l+1}(2V_n)^{2l+1}}{\Gamma(2l+3)}\right\rangle_V. \qquad (3.14)$$

Averaging over the phase one can obtain $\langle a_2\rangle=\left\langle\frac{\epsilon^2}{2V_n^2}\left(\sin(2V_n)-\frac{1}{V_n}(1-\cos(2V_n))\right)\right\rangle_V$, where now $\langle a_2\rangle$is strictly written as function of the average over the velocity variable. One can expand this last expression for $\langle a_2\rangle$in power series and obtain

$$\langle a_2\rangle = \left\langle\frac{\epsilon^2}{V_n^2}\left[V_n+\sum_{l=1}^{\infty}\frac{(-1)^l(2V_n)^{2l+1}}{2\Gamma(2l+2)}-V_n-\sum_{l=1}^{\infty}\frac{(-1)^l(2V_n)^{2l+1}}{\Gamma(2l+3)}\right]\right\rangle_V, \qquad (3.15)$$

and after rearranging properly the terms, we have

$$\langle a_2\rangle = \epsilon^2\left\langle\sum_{l=0}^{\infty}\frac{(-1)^{l+1}\,2\,(2l+2)\,(2V_n)^{2l+1}}{\Gamma(2l+5)}\right\rangle_V. \qquad (3.16)$$

Finally, the average over the last term of eq. (3.12) is given by

$$\left\langle\cos(\phi_n+2V_n)\,a_2-\frac{\sin(\phi_n+2V_n)}{2}a_1^2\right\rangle = 0. \qquad (3.17)$$

To obtain Eq. (3.17), we considered that all third order trigonometric functions, like $\cos^3(\phi_n)$, and their crossed terms, like $\cos(\phi_n)\sin(\phi_n)$, have null averages over the phase variable.

With the previous results obtained in the expressions (3.14), (3.16) and (3.17), one may

write eq. (3.12) as

$$\begin{aligned}\langle V_{n+1}\rangle_V &= \{\gamma\langle V_n\rangle_V\} + \left\{-(1+\gamma)\epsilon^2\left\langle\sum_{l=0}^{\infty}\frac{(-1)^{l+1}(2V_n)^{2l+1}}{\Gamma(2l+3)}\right\rangle_V\right\}m \\ &+ \left\{\gamma\epsilon^2\left\langle\sum_{l=0}^{\infty}\frac{(-1)^{l+1}2(2l+2)(2V_n)^{2l+1}}{\Gamma(2l+5)}\right\rangle_V\right\}m^2. \end{aligned} \tag{3.18}$$

Calculating the auxiliary term $\langle V^{2l}\rangle_V$ as

$$\langle V^{2l}\rangle_V = \int_0^{\infty} V^{2l}\frac{V}{T}e^{-\frac{V^2}{2T}}dV,$$

if we call $u = \frac{V}{\sqrt{2T}}$, we have

$$\begin{aligned}\langle V^{2l}\rangle_V &= \frac{(2T)^{l+1}}{2T}2\int_0^{\infty}u^{2(l+1)-1}e^{-u^2}du, \\ \langle V^{2l}\rangle_V &= (2T)^l\Gamma(l+1), \end{aligned} \tag{3.19}$$

where the gamma function, Γ, is well defined for $l > -1$ [32].

Using eq. (3.19) the expression of the average velocity, eq. (3.18), can then be written as

$$\begin{aligned}\langle V_{n+1}\rangle_V &= \{\gamma\langle V_n\rangle_V\} + \left\{-(1+\gamma)\epsilon^2\sum_{l=0}^{\infty}\frac{(-1)^{l+1}2^{2l+1}(2T)^{l+1/2}\Gamma(l+3/2)}{\Gamma(2l+3)}\right\}m \\ &+ \left\{\gamma\epsilon^2\sum_{l=0}^{\infty}\frac{(-1)^{l+1}2(2l+2)2^{2l+1}(2T)^{l+1/2}\Gamma(l+3/2)}{\Gamma(2l+5)}\right\}m^2, \end{aligned} \tag{3.20}$$

after rearranging properly the terms

$$\begin{aligned}\langle V_{n+1}\rangle_V &= \{\gamma\langle V_n\rangle_V\} + \left\{(1+\gamma)\epsilon^2(8T)^{1/2}\sum_{l=0}^{\infty}\frac{(-8T)^l\Gamma(l+3/2)}{\Gamma(2l+3)}\right\}m \\ &- \left\{2\gamma\epsilon^2(8T)^{1/2}\sum_{l=0}^{\infty}\frac{(2l+2)(-8T)^l\Gamma(l+3/2)}{\Gamma(2l+5)}\right\}m^2. \end{aligned} \tag{3.21}$$

Recalling the following mathematical relation for the gamma function

$$\Gamma(2z) = (\pi)^{-1/2} 2^{2z-1} \Gamma(z) \Gamma\left(z+\frac{1}{2}\right), \tag{3.22}$$

we may obtain after some straightforward algebra

$$\begin{aligned} \sum_{l=0}^{\infty} \frac{(-8T)^l \Gamma(l+3/2)}{\Gamma(2l+3)} &= \frac{\sqrt{\pi}}{4} \sum_{l=0}^{\infty} \frac{(-2T)^l}{\Gamma(l+2)}, \\ &= \frac{\sqrt{\pi}}{8T} \left(1-e^{-2T}\right). \end{aligned} \tag{3.23}$$

The last term of eq. (3.21) stays as $\sum_{l=0}^{\infty} \frac{(2l+2)(-8T)^l \Gamma(l+3/2)}{\Gamma(2l+5)} = \frac{\sqrt{\pi}}{4} \sum_{l=0}^{\infty} \frac{(-2T)^l}{(l+2)(2l+3)\Gamma(l+1)}$. Again, rearranging terms we have

$$\begin{aligned} \sum_{l=0}^{\infty} \frac{(2l+2)(-8T)^l \Gamma(l+3/2)}{\Gamma(2l+5)} &= \frac{\sqrt{\pi}}{4} \sum_{l=0}^{\infty} \left[-\frac{(-2T)^l}{(l+2)\Gamma(l+1)} \right. \\ &\quad \left. + \frac{(-2T)^l}{(l+3/2)\Gamma(l+1)} \right]. \end{aligned} \tag{3.24}$$

To evaluate the sums in eq. (3.24) we use the fact that $\frac{1}{n+1} = \int_0^1 u^n du$, Ref. [33], obtaining thus

$$\begin{aligned} \sum_{l=0}^{\infty} \frac{(2l+2)(-8T)^l \Gamma(l+3/2)}{\Gamma(2l+5)} &= \frac{\sqrt{\pi}}{4} \sum_{l=0}^{\infty} \left[-\frac{(-2T)^l}{\Gamma(l+1)} \int_0^1 u^{l+1} du \right. \\ &\quad \left. + \frac{(-2T)^l}{\Gamma(l+1)} \int_0^1 u^{l+1/2} du \right], \end{aligned} \tag{3.25}$$

then we interchange the order of the summation and the integration. After that, we perform the sum over l

$$\sum_{l=0}^{\infty} \frac{(2l+2)(-8T)^l \Gamma(l+3/2)}{\Gamma(2l+5)} = \frac{\sqrt{\pi}}{4} \left[\int_0^1 e^{-2Tu} u du + \int_0^1 e^{-2Tu} u^{1/2} du \right]. \tag{3.26}$$

Finally, we integrate

$$\sum_{l=0}^{\infty} \frac{(2l+2)\left(-8T\right)^{l}\Gamma\left(l+3/2\right)}{\Gamma\left(2l+5\right)} = \frac{\sqrt{\pi}}{4}\left[-\frac{1}{\left(2T\right)^{2}}+\frac{e^{-2T}}{\left(2T\right)^{2}} + \frac{\sqrt{\pi}}{2\left(2T\right)^{3/2}} erf\left(\sqrt{2T}\right)\right], \tag{3.27}$$

where $erf(x) = \frac{2}{\sqrt{\pi}}\int_0^{\infty} e^{-x^2}dx$ is the error function and is in agreement with $\lim_{x\to\infty} erf(x) = 1$. Therefore, for high temperatures, after replacing eqs. (3.23) and (3.27) in eq. (3.21), making $m = 1$ and putting $\langle V\rangle$in evidence we end up with

$$\langle V\rangle = \frac{1}{1-\gamma}\left[\frac{(1+\gamma)\,\epsilon^2}{2}\sqrt{\frac{\pi}{2T}}+\gamma\epsilon^2\frac{\pi}{4T}\right]. \tag{3.28}$$

The first term on the right does indeed contributes at the limit of high temperatures, then, using eq. (3.7) we find that

$$T = \frac{(1+\gamma)\,\epsilon^2}{2\,(1-\gamma)}, \tag{3.29}$$

which is in remarkable well agreement with the result obtained for the simplified version of the model obtained in eq. (3.4). Similar to discussed for the simplified version, we found also

$$\sqrt{\langle V^2\rangle} = \sqrt{2T}, \tag{3.30}$$

and the deviation around the average velocity

$$\omega = \sqrt{\left(2-\frac{\pi}{2}\right)T}. \tag{3.31}$$

Using Equations (3.7), (3.30), (3.31) and the temperature given by equation (3.29) it is possible to recover similar numerical values for $\langle V\rangle$, V_{rms} and ω shown in Table 2.2, see Table 3.1.

In Table 3.1 we show a comparison for the ω variable regarding analytical results from eqs. (3.6) and (3.4) for the simplified model (ASM), and eqs. (3.31) and (3.29) for the complete model (ACM), with the numerical findings (NSM) and (NCM) respectively, shown in Tables 2.1 and 2.2. One can see that the agreement is relatively good.

ϵ	γ	ω_{ASM}	ω_{NSM}	ω_{ACM}	ω_{NCM}
10	0.999	190.58	197.09(2)	207.12	216.05(1)
100	0.99	601.30	599.91(3)	653.50	653.53(3)
100	0.999	1905.8	1901.5(4)	2071.2	2071.7(2)
100	0.9999	6028	5999(9)	6551	6570(9)
1000	0.999	19058	19054(2)	20712	20706(1)

Table 3.1: Comparison for the ω variable regarding analytical results for the simplified model (ASM) and for the complete model (ACM), with the numerical findings for the simplified approach (NSM) and the complete one (NCM).

Chapter 4

A Monte Carlo approach

In this chapter we present the post-transient mean value of the physical observables in the complete version, eq. (2.7), for a experimentally realizable bouncer model. To do this we introduce a small stochastic noise in the time of flight. We show that the mean values do not strongly depend in the noise size, allowing us to propose a Monte Carlo like simulation that led us to calculate the average values of the observables with great accuracy.

4.1 A Stochastic-Chaotic model

The bouncer model, eq. (2.7), presents the behavior of an ideal particle colliding with a moving platform. In real experiments those deterministic equations are not sufficient to describe the dynamics since there are more variables and physical effects to take into account that influences the behavior of the particle, adding up all those extra phenomena we can consider that the particle suffers a stochastic deviation from its deterministic trajectory.

In this study we add a small stochastic noise in the particle's time of flight. This stochastic noise is of Gaussian type, $\mathcal{N}\left(\mu, \sigma^2\right)$, *i. e.*, we consider in every successive collision the time of flight obtained via eq. (2.8) as a *mean time of flight*, $\mu = t_{v(C)}$, and select an actual $t_{v(S-C)}$, for our Stochastic-Chaotic model, as a random number taken from a Normal distribution along that mean with a specific standard deviation σ, see Figure 4.1, in the case of $t_{v(S-C)} \leq 0$ another value is drawn from the same distribution until $t_{v(S-C)} > 0$. The relation for the time of flight in the Stochastic-Chaotic model is:

$$t_{v(S-C)} \sim \mathcal{N}\left(t_{v(C)}, \sigma^2\right). \tag{4.1}$$

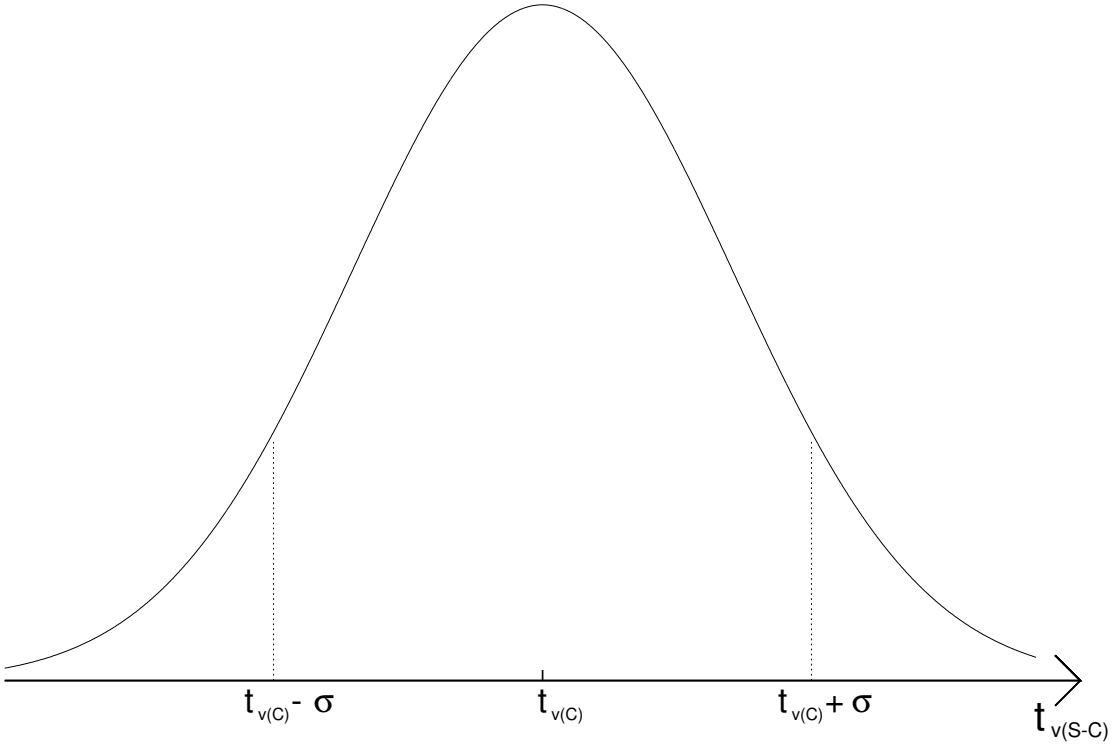

Figure 4.1: The value of time of flight in the Stochastic-Chaotic model, $t_{v(S-C)}$, is a random number of a Gaussian distribution with mean $t_{v(C)}$, solution of equation (2.8), and standard deviation σ.

In Figure 4.2 we show, for different values of σ, the average velocity over an ensemble of orbits as a function of the iteration number n . We can see that all ensembles converge to a stationary state with different rates. However both values, average velocity and crossover time, depend on the value of σ. For bigger σ the convergence to stationary state is achieved more quickly. Also, the convergence value of the velocity appears to grow with σ until it reaches a final value that not longer depends on σ.

The dependence of the final value of the mean velocity, and the root mean square velocity, as function of the parameter σ is better shown in Figure 4.3. At first the value stays almost constant until a crossover σ, where the mean grows rapidly until it reaches a plateau of convergence where the dependence with σ is almost gone. We recall that the Figure 4.3 is in logarithmic scale.

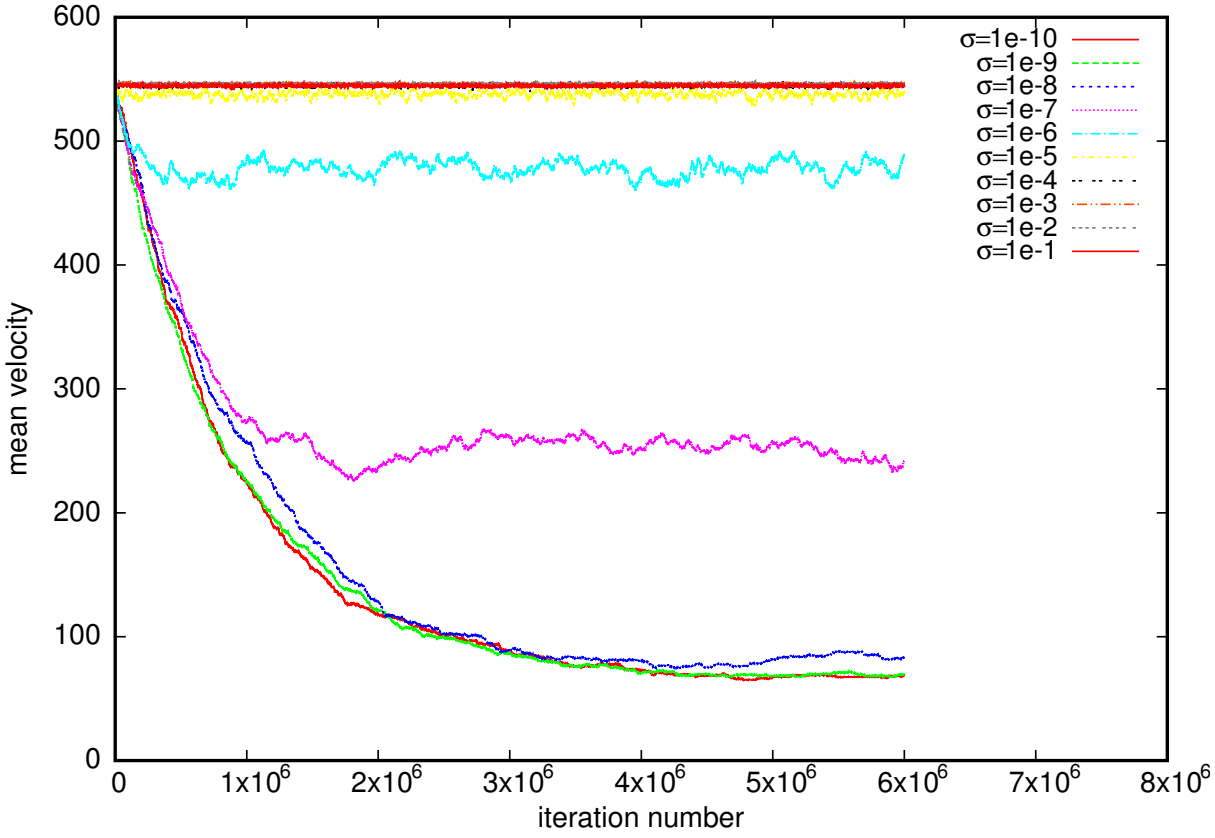

Figure 4.2: Evolution of $\langle V \rangle$ as function of n with σ ranging from 1×10^{-10} to 1×10^{-1}. Al curves show a convergence to a stationary state but for $\sigma > 1 \times 10^{-5}$ the stationary state is almost independent of σ. The control parameters are $\epsilon = 100$ and $\gamma = 0.95$.

For the values of the nonlinear parameter and the dissipation parameter of last section, Table 2.2, the values of $\langle V \rangle$, V_{rms} and others, stay the same for all σ, *i. e.*, both Stochastic and non-Stochastic bouncer model converges to the same stationary state, but for the parameter values used in this section that is not longer true, see Table 4.1 for a comparison of the $\langle V \rangle$ variable, even more, equations (3.7), (3.30), (3.31) are not valid anymore since the phase distribution is not independent of the velocity.

ϵ	γ	$\langle V \rangle_C$	$\langle V \rangle_{S-C}$
10	0.999	407.50(8)	413.25(7)
100	0.999	3959.7(1)	4021.0(3)
1000	0.999	39608(9)	39492(5)
10	0.95	11.621(6)	54.754(6)
100	0.95	69.156(4)	545.15(2)
1000	0.95	640.97(3)	5445.2(1)

Table 4.1: Comparison for the $\langle V \rangle$ variable regarding the Chaotic model (C) and the Stochastic-Chaotic model (S-C).

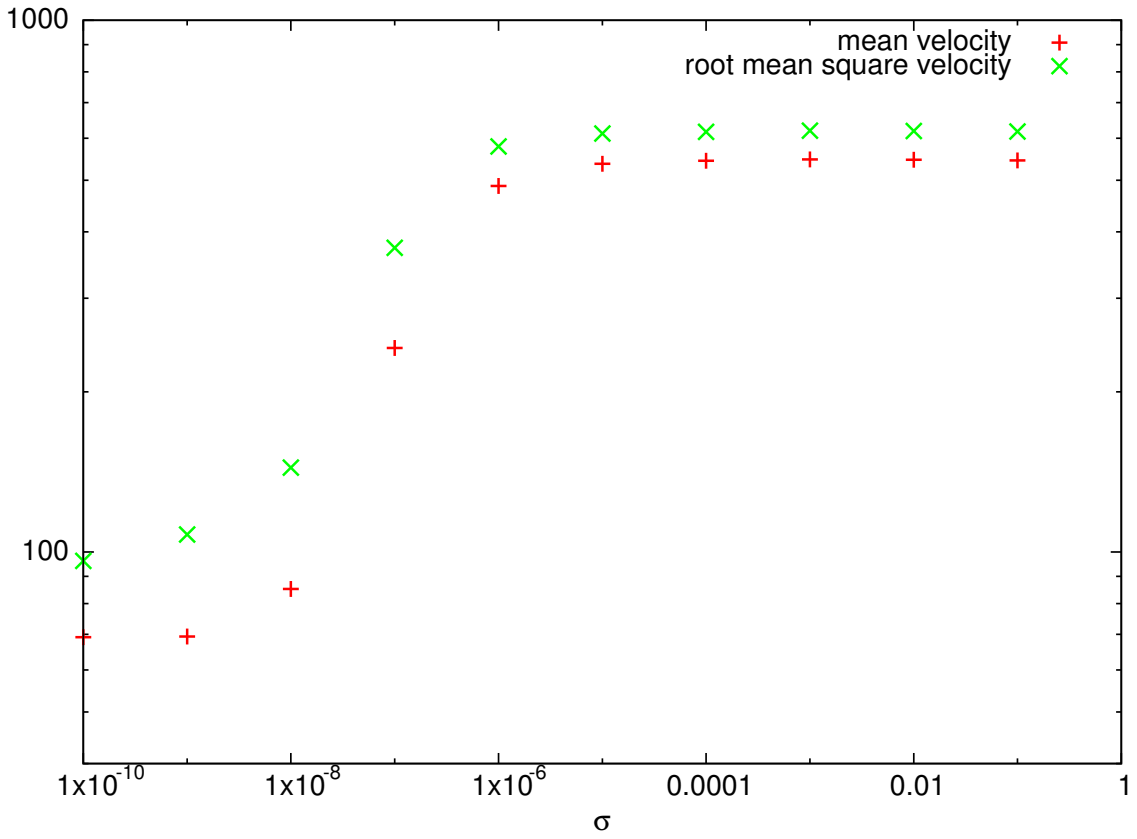

Figure 4.3: Final value of $\langle V \rangle$ and V_{rms} as function of σ with control parameters are $\epsilon = 100$ and $\gamma = 0.95$. for $\sigma > 1 \times 10^{-5}$ there is a plateau.

4.2 Monte Carlo approach

It was shown in last section that the Stochastic-Chaotic model achieves an equilibrium state independent for a large noise range, with this in consideration we develop a kind of Monte Carlo simulation to search averages in a more rapidly form. To do this we proceed in the following way: After every collision the particle's trajectory can have the next collision with the border in three different forms: (i) a tangential way, the particle velocity is the same as the wall velocity when colliding; (ii) a sub-tangential way, the velocity of the particle after the first collision is less than the velocity necessary for second collision be a tangential one; and (iii) a sup-tangential way, the velocity of the particle is more than the one needed for a tangential collision, see Figure 4.4. After classifying the kind of collision, we find a domain of time where next collision can happen. Then we draw a random number from that domain of time to propose a time of flight for the collision. Since it is not an actual calculation, equation (2.8) is not accomplished, but we are able to find how far from zero is the value, *i. e.*, how far are the particle and the wall for the proposed time of flight. The idea is to accept the collision with a probability that grows as the distance from the particle to the wall goes to zero. If the time of flight is rejected we propose another time and proceed once again.

The tangential velocity condition for any phase can be calculated remembering that before

the tangential collision both particle and wall have the same velocity, then we reverse the time in the dynamics and find which initial conditions lead to that tangential collision. If the tangential velocity condition is known for some phases, then for any phase, the velocity, which leads to a tangential collision, can be calculated via interpolation. With that in mind we have to do a few of actual simulations and store the data, which is used to know, via interpolation, if our velocity, for a given phase, would leave to a sub-tangential, tangential or sup-tangential collision.

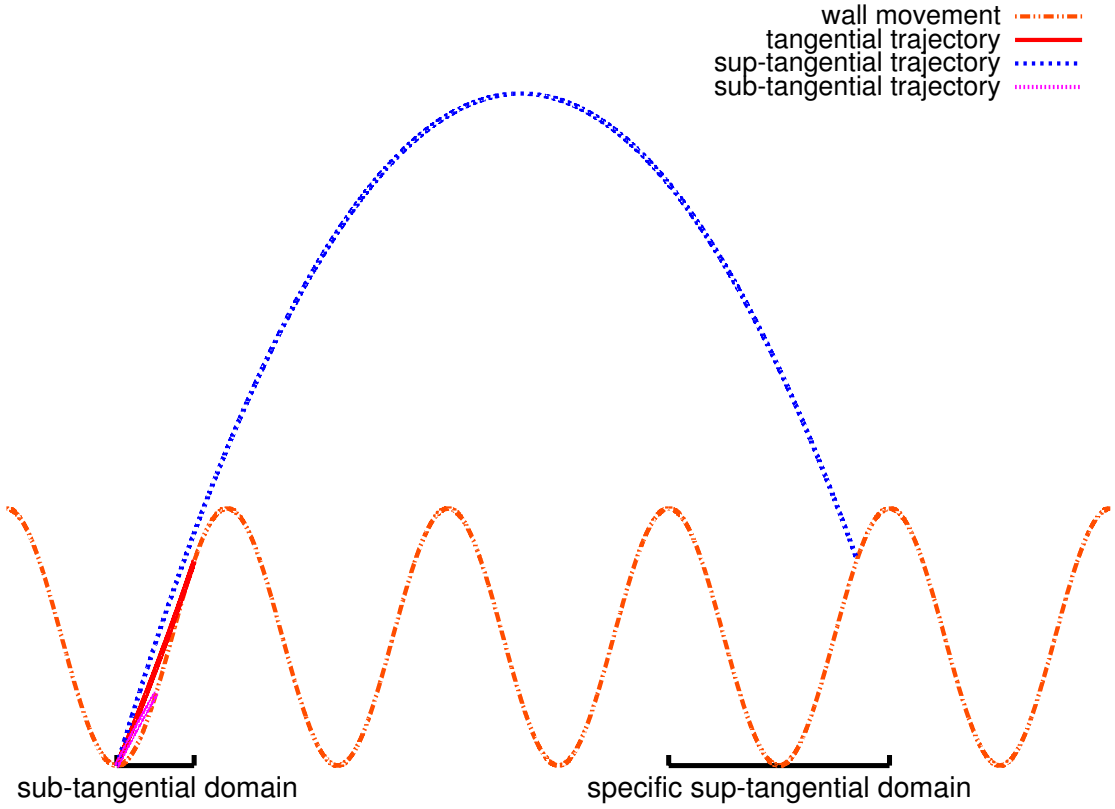

Figure 4.4: Classification of trajectories of the complete bouncer model, each kind of trajectory has its proper domain for piking randomly the time of flight.

In a numerical simulation the probability to have a tangential collision is almost zero. So we needed to worry about the other kinds of collisions, if it was known that the collision would be sub-tangential, with the interpolation analysis described before, we pick a random number for the time o flight between zero and the time of flight for a tangential collision.

If the collision is known to be sup-tangential then we calculate the number of oscillations n that the wall goes until next collision. To do this we remember that the trajectory of the particle is described by

$$x_f = x_0 + Vt - \frac{t^2}{2}, \tag{4.2}$$

where $x_0 = \epsilon \cos(\phi)$, the final position is $x_f = \epsilon$, see Figure 4.4 where the specific subdomain

is between two maxima of position, and the time elapsed to reach that position is $t = 2n\pi - \phi$. Recall that ϕ and V give the phase and velocity of the current collision. So the final inequation that relates the number of oscillations, n, in terms of ϕ and V is

$$\frac{2n\pi - \phi}{2} - \frac{\epsilon\left(\cos\left(\phi\right) - 1\right)}{2n\pi - \phi} < V < \frac{2\left(n+1\right)\pi - \phi}{2} - \frac{\epsilon\left(\cos\left(\phi\right) - 1\right)}{2\left(n+1\right)\pi - \phi}. \tag{4.3}$$

The idea is to find an integer n in such way that the given V fulfills the last inequation. With the value of n is possible to define a specific finite domain for the time of flight $[2n\pi, 2\left(n+1\right)\pi]$ from where we draw a random number.

Once we draw a random time of flight, t_v, we use equation (2.8) to calculate $G\left(t_v\right)$. With this value we either accept or reject the proposed time t_v. The acceptance/rejection decision is done in a *Monte Carlo* style. We calculate

$$P = e^{-\frac{\left(G(t_v)\right)^2}{2\beta^2}}, \tag{4.4}$$

were β is a parameter introduced to control the acceptance/rejection ratio. Then draw a random number, from a uniform distribution between $[0, 1]$, and ask whether the random number is greater (or smaller) than P. If it is greater we draw another random time of fight t_v, other case we accept the time of flight and the respective collision and proceed once again.

The method proposed for the Monte Carlo simulation has some resemblance with the actual method for the Chaotic model. While in the later we *propose* a new time of flights via particle dynamics, and use the acceptance/rejection probability distribution shown in Figure 4.5, in the former we *propose* a new time of flight in the described manner, and use the acceptance/rejection probability distribution given by equation (4.4), see Figure 4.6.

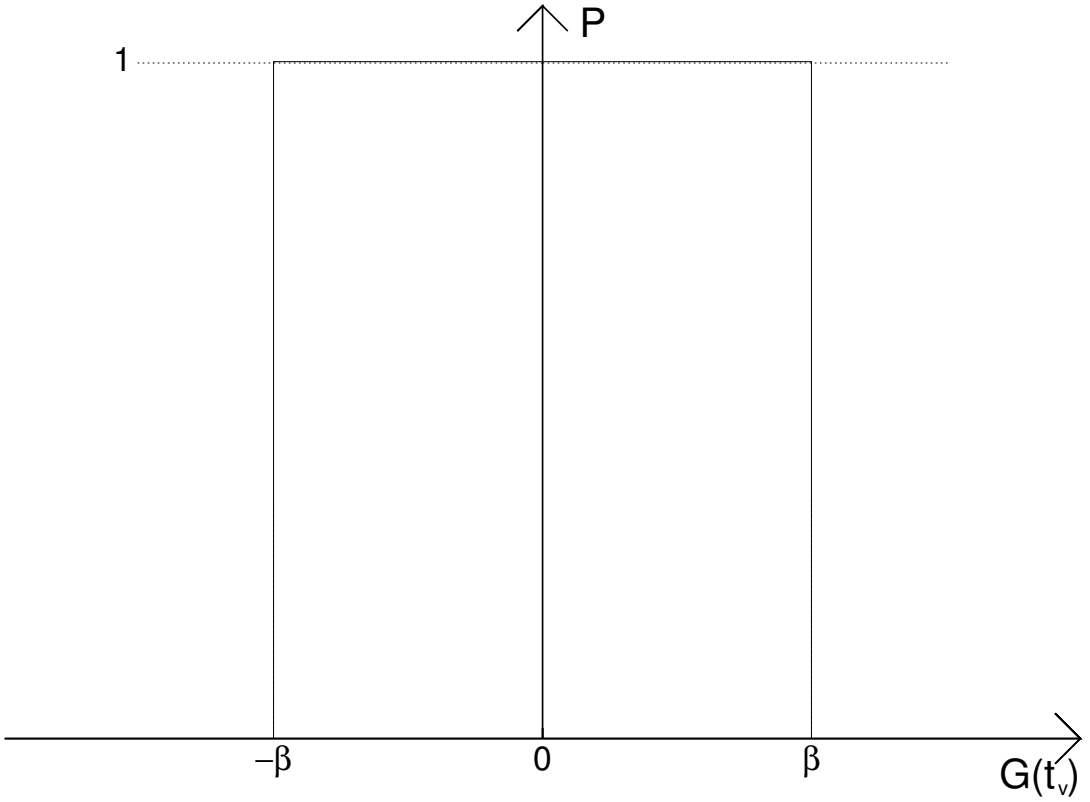

Figure 4.5: Acceptance/rejection probability distribution as function of $G\left(t_v\right)$ for the Chaotic simulation. In an algorithm in double precision machine usually $\beta = 1 \times 10^{-14}$.

We see in Table 4.2 that with the Monte Carlo simulation we found similar results to ones obtained by the Stochastic Chaotic model, given robustness to the proposed method.

ϵ	γ	$\langle V \rangle_{M-C}$	$\langle V \rangle_{S-C}$
10	0.999	405.26(9)	413.25(7)
100	0.999	3946.4(5)	4021.0(3)
1000	0.999	39352(3)	39492(5)
10	0.95	52.890(9)	54.754(6)
100	0.95	529.22(7)	545.15(2)
1000	0.95	5295.7(2)	5445.2(1)

Table 4.2: Comparison for the $\langle V \rangle$ variable regarding the Monte Carlo simulation (M-C) and the Stochastic-Chaotic model (S-C).

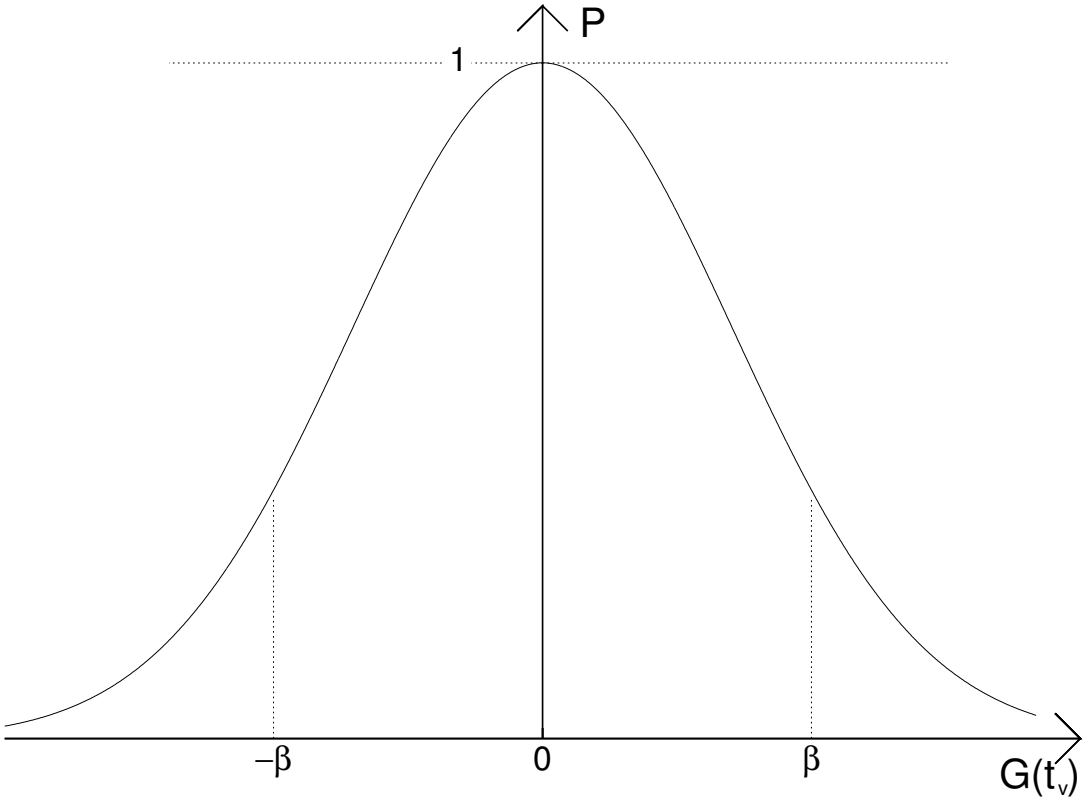

Figure 4.6: Acceptance/rejection probability distribution as function of $G\left(t_v\right)$ for the Monte-Carlo simulation. In the numerical simulation we used $\beta \propto \epsilon$.

Chapter 5

Conclusions and perspectives

The dynamics of a dissipative 1-D impact system was described by nonlinear mappings for two different versions, complete and simplified, for the velocity of the particle and the phase of the vibrating wall. Dissipation was introduced via inelastic collisions leading to the existence of attractors in the phase space.

A numerical and statistical investigation for the variables $\langle V \rangle$, V_{rms} and ω (deviation of the average velocity) was made for both versions of the mappings. For long time series, these observables bend towards a saturation plateau which marks the stationary state. Such a regime varies as the control parameters associated with the dissipation (γ) and the nonlinear parameter (ϵ) are changed.

We developed a new semianalytic method to obtain algebric equations for the $\langle V \rangle$, V_{rms} and ω variables in the equilibrium state as functions of the parameters of the model, with these equations we were able to calculate the numerical values of those variables without doing the simulations. A remarkable assembly was obtained considering both numerical and theoretical investigations, between statistical and thermal variables.

When introducing a Stochastic Gaussian noise, with a standard deviation σ in the time of flight, we found that the system achieves a thermal equilibrium for every σ, and for large enough noise, this equilibrium was independent of the noises size perturbation. This phenomenon allowed us to propose a Monte Carlo scheme for simulating a stochastic bouncer model in which the numerical simulation was faster and achieved the similar results for the observables $\langle V \rangle$, V_{rms} and ω as the ones found with the original simulation for the stochastic bouncer model.

All results show robustness in the formalism and simulation approach, as a perspective this opens 'new doors' for similar analysis in other more complex dynamical systems, particularly in time dependent billiards.

Bibliography

[1] Newton, Isaac. *Philosophiae Natvralis Principia Mathematica*. Characteribvs Caesareo-Regiae Scholae Normalis, Per Ioannem Adamvm Hagen, Factorem, (1780).

[2] Poincaré, Henri. *Les méthodes nouvelles de la mécanique céleste*. Gauthier-Villars it fils, (1892-1899)

[3] Sundman, Karl F. *Mémoire sur le problème des trois corps*. Acta mathematica 36.1 (1913): 105-179.

[4] Qiu-Dong, Wang. *The global solution of the n-body problem*. Celestial Mechanics and Dynamical Astronomy 50.1 (1990): 73-88.

[5] Diacu, Florin. *The solution of the n-body problem*. The Mathematical Intelligencer 18.3 (1996): 66-70.

[6] Lorenz, Edward N. *Deterministic nonperiodic flow*. Journal of the atmospheric sciences 20.2 (1963): 130-141.

[7] Feigenbaum, Mitchell J. *The universal metric properties of nonlinear transformations*. Journal of Statistical Physics 21.6 (1979): 669-706.

[8] Strogatz, Steven H. *Nonlinear dynamics and chaos: with applications to physics, biology, chemistry, and engineering*. Westview press, (2014).

[9] R. C. Hilborn, *Chaos and Nonlinear Dynamics: An Introduction for Scientists and Engineers*. Oxford University Press, New York, (1994).

[10] A. J. Lichtenberg, M.A. Lieberman, *Regular and Chaotic Dynamics*. Appl. Math. Sci. 38, Springer Verlag, New York, (1992).

[11] G. M. Zaslasvsky, *Physics of Chaos in Hamiltonian Systens*. Imperial College Press, New York (2007).

[12] G. M. Zaslasvsky, *Hamiltonian Chaos and Fractional Dynamics*. Oxford University Press, New York (2008).

[13] Bunimovich, Leonid Abramovich. *On ergodic properties of certain billiards*. Functional Analysis and Its Applications 8.3 (1974): 254-255.

[14] Chernov, Nikolai, and Roberto Markarian. *Chaotic billiards*. No. 127. American Mathematical Soc., (2006).

[15] Dettmann, Carl P. *Recent advances in open billiards with some open problems*. Frontiers in the Study of Chaotic Dynamical Systems with Open Problems 16 (2011): 195.

[16] Birkhoff, George D. *On the periodic motions of dynamical systems*. Acta Mathematica 50.1 (1927): 359-379.

[17] Sinai, Yakov Grigor'evich. *Dynamical systems with elastic reflections*. Russian Mathematical Surveys 25.2 (1970): 137-189.

[18] Krylov, Nikolai Sergeevich. *Works on the foundations of statistical physics*. Princeton University Press, (1979).

[19] R. K. Pathria, *Statistical Mechanics*. Elsevier - Burlington (2008).

[20] M.E.J. Newman, G.T. Barkema, *Monte Carlo Methods in Statistical Physics*. Oxford Unifersity Press Clarendon, New York (2001).

[21] Pustyl'nikov, Lev Davidovich. *On Ulam's problem*. Theoretical and Mathematical Physics 57.1 (1983): 1035-1038.

[22] Karlis, A. K., et al. *Hyperacceleration in a stochastic Fermi-Ulam model*. Physical review letters 97.19 (2006): 194102.

[23] Fermi, Enrico. *On the origin of the cosmic radiation*. Physical Review 75.8 (1949): 1169.

[24] Leonel, Edson D., and André LP Livorati. *Describing Fermi acceleration with a scaling approach: the Bouncer model revisited*. Physica A: Statistical Mechanics and its Applications 387.5 (2008): 1155-1160.

[25] Livorati, André Luis Prando, Denis Gouvêa Ladeira, and Edson D. Leonel. *Scaling investigation of Fermi acceleration on a dissipative bouncer model*. Physical Review E 78.5 (2008): 056205.

[26] Tavares, Danila F., Edson D. Leonel, and R. N. Costa Filho. *Non-uniform drag force on the Fermi accelerator model*. Physica A: Statistical Mechanics and its Applications 391.22 (2012): 5366-5374.

[27] Tavares, Danila F., et al. *Dynamical properties for a mixed Fermi accelerator model*. Physica A: Statistical Mechanics and its Applications 392.19 (2013): 4231-4241.

[28] Leonel, Edson D., et al. *A dynamical phase transition for a family of Hamiltonian mappings: A phenomenological investigation to obtain the critical exponents*. Physics Letters A 379.32 (2015): 1808-1815.

[29] Oliveira, Diego FM, Mario Roberto Silva, and Edson D. Leonel. *A symmetry break in energy distribution and a biased random walk behavior causing unlimited diffusion in a two dimensional mapping*. Physica A: Statistical Mechanics and its Applications 436 (2015): 909-915.

[30] Leonel, Edson D., and André LP Livorati. *Thermodynamics of a bouncer model: A simplified one-dimensional gas*. Communications in Nonlinear Science and Numerical Simulation 20.1 (2015): 159-173.

[31] N. L. Johnson, S. Kotz, N. Balakrishnan, *Continuous Univariate Distributions*. Volume 1, Second Edition, Jonh Wiley and Sons (1995)

[32] George B. Arfken *Mathematical Methods for Physicists*. Third Edition, Academic Press Inc. (1985).

[33] R. B. Dingle *Asymptotic Expansions: Their Derivation and Interpretation*. Academic Press, (1973).